JCTC Journal of Chemical Theory and Computation

Article

pubs.acs.org/JCTC

Water-Driven Cavity–Ligand Binding: Comparison of Thermodynamic Signatures from Coarse-Grained and Atomic-Level Simulations

Riccardo Baron*,† and Valeria Molinero*,‡

†Department of Medicinal Chemistry, College of Pharmacy, and The Henry Eyring Center for Theoretical Chemistry, The University of Utah, Salt Lake City, Utah 84112-5820, United States

‡Department of Chemistry and The Henry Eyring Center for Theoretical Chemistry, The University of Utah, 315 South 1400 East, Salt Lake City, Utah 84112-0850, United States

Supporting Information

ABSTRACT: The role of water (thermo)dynamics is crucial in molecular recognition and self-assembly. Here, we study a prototype cavity–ligand system as a model for hydrophobic noncovalent binding. Two alternative molecular dynamics simulation resolutions are employed and the resulting structural, dynamic, and thermodynamic properties compared: first, a coarse-grained (CG) resolution based on the previously reported and validated methane-like M solute and mW water models; second, an atomic-level (AL) resolution based on the popular OPLS united atom methane and the TIP4P water models. The CG model reproduces, as a function of the cavity–ligand distance, (1) the water occupancy of the cavity, (2) the cavity–ligand potential of mean force (free energy) and its temperature dependence, and (3) some of the major qualitative features of the thermodynamic signatures (free energy, enthalpy, and entropy) for cavity–ligand association of the AL model. The limits of the CG and AL models in this context are also discussed with comparison to experimental data. Our study suggests that CG simulation with models that include the translational contribution of water and anisotropic "hydrogen-bond"-like interactions could reproduce the thermodynamics of molecular recognition and water-driven assembly in complex macromolecular systems and nanoscale processes with convenient computational time savings.

1. INTRODUCTION

Water is the most important solvent for life, and molecular recognition plays a role in molecular sciences that cannot be overemphasized. The role of water for protein stability and dynamics has been well-known since the pioneering molecular dynamics (MD) simulations of fully solvated protein systems by van Gunsteren and Berendsen.[1,2] However, the general observation that water appears to be a major, active player as well in noncovalent molecular binding has been taking shape only more recently. MD simulation studies of model systems have proposed that cavity–ligand association could indeed be driven by water-related contributions.[3,4] The counterintuitive observation that water-related interactions may dominate over the direct ligand–cavity interaction has broad implications for understanding virtually all molecular association processes occurring in solution and is expected to be highly transferable to biologically relevant scenarios.[5] For example, it is most crucial to predict and improve drug-binding affinities.[6−8]

The thermodynamic role of solvent fluctuations in nanoscopic hydrophobic cavities resulting from wetting/dewetting transitions[9,10] could be particularly relevant in this context. Concave cavities on the surface of complex biomolecular systems are typical host sites for drug-like ligands, which favorably associate while presenting large and almost compensating enthalpy and entropy terms.[11] A thermodynamic penalty has to be paid to remove these highly entropic, favorable fluctuations upon ligand association. The water expelled from a cavity forms new interactions in the bulk that could compensate for this loss in entropy.[3,4] Therefore, not only water binding propensities[12−14] but also water fluctuations may be of importance to predict noncovalent binding free energies and their temperature dependence. Nevertheless, accessing reversible wetting/dewetting using MD simulation along the spatiotemporal scales involved (typically nanoscale and hundreds of nanoseconds) is still often prohibitively expensive, and the sampling problem[15] limits the possibility to collect reliable statistics on solvent fluctuations. In this article, we focus on model cavity–ligand systems and explore the properties of a coarse-grained (CG) model with explicit solvent as a valid alternative to popular atomic-level (AL) models to capture solvent (thermo)dynamics in molecular recognition.

On one hand, simplified CG models with explicit solvent are extremely attractive for computer simulation, because at least 80% of the simulation time for solvated macromolecules is typically dedicated to the calculation of water-related interactions. CG MD, at the cost of spatiotemporal resolution, cuts computational load in two distinct ways. First, by reducing the number of system degrees of freedom the machine time requires to perform one MD step shortens. Second, CG potentials are typically smoother, allowing for longer MD integration time steps.[16] Additionally, some CG potentials may include *ad hoc* simplifications, such as shorter interaction cutoff

Special Issue: Wilfred F. van Gunsteren Festschrift

Received: February 9, 2012
Published: June 5, 2012

   dx.doi.org/10.1021/ct300121r | *J. Chem. Theory Comput.* 2012, 8, 3696–3704

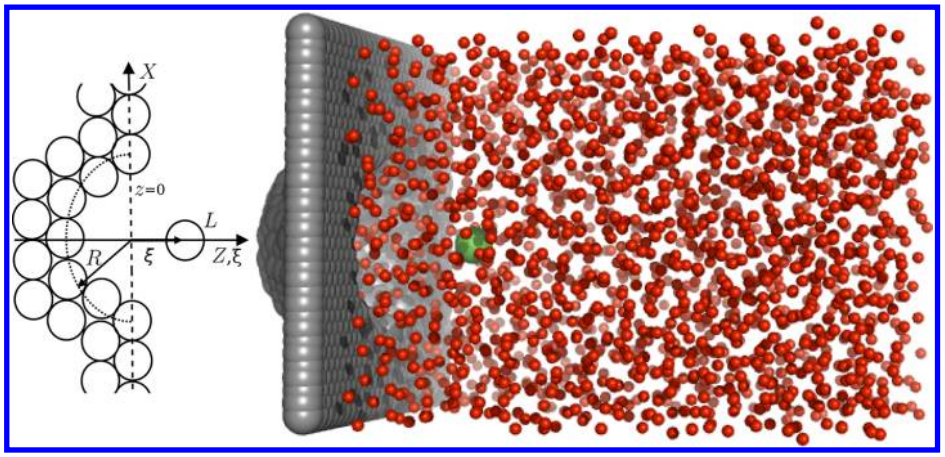

Figure 1. Schematic representation and snapshot of the studied system with highlighted hydrophobic hemispherical cavity (radius R = 0.8 nm, gray) and hydrophobic ligand (L, green). The system is explicitly solvated with mW coarse-grained (CG) water particles (red). A corresponding atomic-level (AL) system was simulated using the TIP4P water model (not shown). Note that $\xi = 0$ corresponds to the wall surface.

lengths and/or elimination of electrostatic interactions to further speed up computation. As a result, CG and AL time scales are not directly comparable. It was shown that mapping CG and AL MD time scales is possible using entropy as a measure of the phase space accessed at different model resolutions.[17,18]

On the other hand, the ability of CG force fields to reproduce experimental and/or AL thermodynamics has been explored, and although one can match free energies between different model resolutions, a reduction of the number of degrees of freedom can be expected to lead to nonphysical reduction of the entropy and nonphysical entropy−enthalpy compensation. Consistently, only CG models with a resolution higher than three water molecules per bead have been reported to simultaneously capture various macrosopic properties of water.[19] For example, a general weaker dependence of physical properties on the temperature and a reduced heat capacity have been expected and reported for CG models in which more aggressive coarse graining is employed.[17,20] However, it is possible to limit this nonphysical consequence of model coarse graining to the rotational component of a liquid by using water models that represent one water molecule per bead. As for any modeling decision, whether this is crucial or irrelevant mainly depends on the goals one defines when developing and applying a CG force field. Indeed, when effective beads represent more than one water molecule per bead, coarse graining leads intrinsically to both rotational and translational entropy losses.

Here, we investigate the use of an explicit solvent CG model to capture the qualitative behavior of solvent dynamics and molecular recognition thermodynamics. We study Setny et al.'s model system[3,21−24] as a prototype of hydrophobic cavity−ligand binding (Figure 1). We employ the apolar mW water model that effectively represents each water molecule as a single particle with anisotropic "hydrogen-bonding" tetrahedral interactions.[25] The mW model reproduces the radial and angular distribution function of the oxygen atoms in liquid water, the liquid−vapor surface tension, the density of the liquid, and its vaporization enthalpy under standard conditions with a precision comparable to that of most popular AL water models.[25,26] The mW model also reproduces the thermodynamic, structural, and dynamical anomalies of liquid water[25,27] and phase transitions between liquid and ice[28,29] and liquid and clathrate hydrates[30−32] with a computational time savings of at least 2 orders of magnitude.[25]

Of particular relevance for the present study, the mW CG model captures the thermodynamic behavior of water-mediated interactions between pairs of either *large* or *small* length-scale hydrophobes. The Setny's cavity of interest herein mixes these two extreme length scales, with peculiar thermodynamic implications that have been extensively discussed.[3,8] For example, mW was used to characterize the thermodynamics and dynamics of wetting/dewetting transitions between nanoscopic hydrophobic plates[33] and of the potential of mean force of a methane pair as a function of the temperature.[30,32,34] The potential of mean force for a pair of coarse-grained methane molecules (M particles) in mW water (Supporting Information, Figure S1) is close to that for a pair of OPLS methane molecules in TIP4P water.[35] The association of the methane molecules in mW is enhanced at high temperatures, indicating that methane−methane association in mW to form a contact pair is driven by entropy,[30] as predicted by atomistic models. Pascal et al. have recently shown that the mW model reproduces the thermodynamic signatures (free energy, enthalpy, and entropy) of atomistic water in hydrophobic carbon nanotubes.[37] On the contrary, the W/M3B potential that represents water as a single particle interacting through isotropic Morse potentials[36] does not reproduce the thermodynamic signatures of the atomistic water model.[37]

In this work, we calculate the thermodynamic signatures of the noncovalent binding process between a hemispherical cavity and a ligand using the CG model based on mW water and the methane-like M solute[30,32,34] and compared it with AL data based on the popular TIP4P water model[38] and the OPLS united-atom methane model.[39] We find that the CG model accurately reproduces as a function of the cavity−ligand distance (1) the water occupancy of the cavity, (2) the cavity−ligand potential of mean force and its temperature dependence, and (3) the major qualitative features of the thermodynamic signature for cavity−ligand association of the AL model. Overall, our study shows that CG simulations could provide a promising approach to capturing the qualitative features of molecular recognition thermodynamics, including solvent fluctuations and enthalpy−entropy compensation. This study sets the basis for future extensions of the use of the mW

water model to complex biomolecular association and water-driven assembly.

2. MOLECULAR MODELS AND METHODS

The simulated systems were larger versions of Setny's model system (Figure 1),[3,21−24] constituted by one hemispherical cavity of 0.8 nm radius embedded in a rectangular paraffin-like wall of dimensions 3.5 × 3.3 nm, constructed as a hexagonal close packed (HCP) grid of lattice constant 0.125 nm and filled with 1950 water molecules, resulting in a box with edge $z \approx 5.4$ nm from the cavity wall. The hemispherical paraffin wall and cavity contain 3360 and 4242 (positionally constrained) particles in the CG and AL simulations, respectively. These differences arise from the fact that a trimmed cavity was employed in the CG system, thus containing fewer layers of paraffin particles on the external side of the wall that is not in direct contact with water. The reaction coordinate ξ for the determination of the free energy is the distance between the ligand and the plane of the cavity wall surface (located at $\xi = 0$; Figure 1). Negative ξ values correspond to the ligand inside the cavity. Periodic boundary conditions were enforced in the x,y directions only. A 9−3 LJ (CG) or harmonic (AL) potential wall was applied to avoid water evaporation on the side opposite the cavity and to reproduce the experimental average density of liquid water in the middle of the simulation box (0.1% tolerance). Table 1 summarizes the simulation systems and the parameters used.

Table 1. Summary of the Systems and Parameters Used for MD Simulation[a,b]

	CG	AL
no. paraffin (P) particles	3360	4242
no. water (W) particles	1950	1950
no. ligand (L) particles	1	1
P−L	LJ(ε_{PL} = 0.0543; σ_{PL} = 0.3941)[c,e]	
P−W	LJ(ε_{WL} = 0.0628; σ_{WL} = 0.3652)	LJ(ε_{WL} = 0.0395; σ_{WL} = 0.3652)[c,e]
W−L	SW(ε_{WL} = 1.004; σ_{WL} = 0.405) M[f]	LJ(ε_{WL} = 0.8934; σ_{WL} = 0.3441)[c,d]
W−W	SW(2- and 3- body terms) mW[g]	LJ(ε_{WW} = 0.6489; σ_{WW} = 0.3153)[c,d]

[a]CG nonbonded LJ interaction cutoff was set to 1.1 nm; AL nonbonded interaction cutoff was smoothly shifted to zero at 1.2 nm using VSHIFT in CHARMM.[45] [b]Energies in kJ mol^{-1}; lengths in nm. [c]Lennard-Jones potential: $U_{LJ}(r_{ij}) = 4\varepsilon_{ij}(\sigma_{ij}/r_{ij})^{12} - (\sigma_{ij}/r_{ij})^{6})$. [d]OPLS force field[38,39] and TIP4P water model[38] and applying standard Lorenz-Berthelot mixing rules: $\varepsilon_{ij} = (\varepsilon_{ii}\cdot\varepsilon_{jj})^{1/2}$ and $\sigma_{ij} = (\sigma_{ii} + \sigma_{jj})/2$. For TIP4P, we refer to the OT interaction site. [e]The hydrophobic wall is modeled in order to reproduce a paraffin-like material of 0.8 g cm^{-3} density, composed of CH_2 units. Note that identical parameters were employed for both CG and AL simulations. See the supporting information in ref 3. [f]Stillinger-Weber potential (2 body term) as in the methane-like M particle from refs 30, 32, and 34. [g]Stillinger-Weber potential (2 and 3 body terms) as in the mW water model from ref 25.

In the CG system, water molecules were modeled as mW particles[25] interacting through two- and three-body energy terms in the form of a Stillinger-Weber (SW) potential.[40] The ligand was modeled as an M particle which interacts with water through a two-body, isotropic, SW potential.[30,32,34] A summary of the model parameters is given in Table 1. CG simulations were generated with LAMMPS[41] in the *NVT* ensemble, integrating Newton's equations of motion[42] with a time step of 5 fs and by maintaining the average system temperature with the Nosé−Hoover extended-ensemble thermostat.[43,44] In the AL system, the TIP4P water model was used,[38] and the ligand was modeled as one neutral LJ sphere with OPLS methane parameters.[38,39] New AL simulations in the *NVE* ensemble and previously reported simulations in the *NVT* ensemble were performed with CHARMM[45] integrating Newton's equations of motion[42] with a time step of 1 fs. The new simulations performed on the larger system presented here (1950 vs 1030 water molecules) display ensemble average intensive properties virtually identical to those previously reported in ref 3.

The interaction potential between paraffin sites and ligands (P−L) is a 6−12 Lennard-Jones (LJ) potential with identical parameters (Table 1) in the coarse-grained (CG) and atomic-level (AL) systems. In both the CG and AL systems, the paraffin particles of the cavity interact with the ligand through 6−12 LJ potentials that reproduce the hydrophobicity of a paraffin-like material. We refer the reader to Table 1 and the supporting information of ref 3 for details of the AL cavity−water interaction. The characteristic size σ of the 6−12 LJ P−W potential is the same in the CG and AL models, while the characteristic energy ε was tuned to produce roughly the same average water occupancy in the cavity in the absence of methane. The hydrophobicity of the cavity with respect to the CG mW water is evinced in a contact angle larger than 90° for a droplet of mW water simulated at 298 K over a flat paraffin-like surface that constitutes the cavity and its wall (see Supporting Information, Figure S2). We note that, mostly due to the different paradigms upon which the AL and CG models are built,[25] and also due to the fact that the cavity was trimmed in the CG simulations, different values of ε for the P−W interaction are needed to match the same average values of water occupancy in the cavity in the absence of a ligand.

Water molecules (AL: water oxygen) falling beyond $z < 0$ (wall distance) were considered to be inside the cavity. The results presented are essentially independent of minor variations of this arbitrary criterion. Free energy changes along the cavity−ligand binding coordinate, ξ, were estimated differently for CG and AL simulations. For the CG system, the free energy was computed from the direct integration of the forces on the ligand along z, $G(\xi) = -\int_{\xi_U}^{\xi}\langle F_z\rangle\,dz$, where each $\langle F_z\rangle$ is the ensemble averaged z component of the force on the ligand constrained at a distance ξ over a (10−80-ns-long) *NVT* simulation, ξ_U =1.5 nm corresponds to an unbound ligand−cavity state in which no anisotropic forces act on the ligand. The integration was performed from simulations in the range $-0.48 < \xi < 1.5$ nm with the ligand constrained at a discrete position separated by 0.02 nm. CG simulations were performed along this ξ range at five temperatures, T = 278, 298, 308, 318, and 338 K, yielding more than 600 independent *NVT* simulations totaling about 20 μs. For the AL system, $G(\xi)$ was determined through umbrella sampling and WHAM reweigthing from *NVT* simulations at T = 298, 308, 318, 328, and 338 K as detailed in ref 3. For CG and AL simulations, the entropy and enthalpy contributions to the free energy, $S(\xi)$ and $H(\xi)$, were obtained from the temperature dependence of $G(\xi)$ as described in ref 3.

Liquid−vapor surface tensions γ_{lv} of mW water at temperatures ranging from 250 to 350 K were computed using the systems and protocols detailed in ref 25. The surface entropy

was computed from the temperature derivative of γ_{lv} at constant pressure, $S_s = -(\partial\gamma_{lv}/\partial T)_p$. The derivative was determined analytically after fitting γ_{lv} to a second order polynomial of T.

3. RESULTS AND DISCUSSION

3.1. Hydration and Dewetting Transitions at CG and AL Resolutions. We analyzed the correspondence between coarse-grained (CG) and atomic-level (AL) simulation results starting from the hydration of the hydrophobic cavity and its changes upon moving the hydrophobic ligand, L, along the binding coordinate, ξ (Figure 1). These results are summarized in Figure 2 in terms of water occupancy inside the cavity as a function of ligand distance from the wall surface located at ξ = 0. A remarkable correspondence between CG and AL models can be observed. First, the two models present a similar number of water molecules inside the cavity as a function of ξ. As the ligand approaches the wall, the water content in the cavity increases with a maximum in both models at about ξ = 0.6 nm, followed by a sudden dewetting of the cavity when the ligand is at about 0.4 nm. A minimum hydration is observed when the ligand is just outside the cavity (0 < ξ < 0.2 nm) followed by small rise in the hydration of the cavity as the ligand approaches the cavity bottom. Second, the corresponding standard deviation values of the fluctuations of the number of water molecules in the cavity are close in the CG and AL models. These results also show that the CG model parameters used to represent cavity−water interactions (Table 1) are in line with the hydrophobic properties of the Setny et al.'s cavity system.[21,22,24]

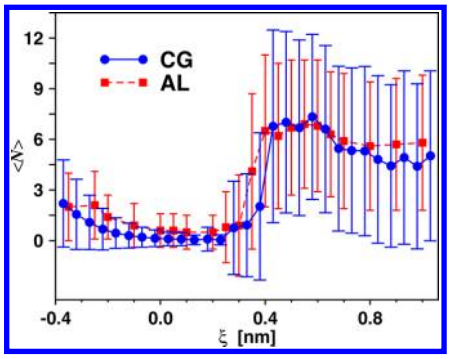

Figure 2. Hydration of the hydrophobic cavity as a function of ligand distance from the paraffin wall. Values of the average number of coarse-grained (CG, blue) or TIP4P (AL, red) water molecules in the cavity (ξ < 0) are shown along the cavity−ligand binding coordinate ξ. Vertical bars represent the standard deviation values, which evidence wetting/dewetting transitions when the ligand is outside the cavity.

The role of solvent fluctuations within the cavity and their removal upon binding are aspects of particular relevance for the entropy and enthalpy contributions to cavity−ligand binding thermodynamics.[3,4] Figure 3 summarizes the comparison between CG and AL models for the cavity−ligand scenario in which these fluctuations are more pronounced, that is the situation in which the ligand is at a far distance from the cavity (ξ = 1.15 nm). In this case, one CG run (50 ns) and two independent AL runs (20 ns each) were employed, to achieve improved statistics. The average occupancy of the cavity is only slightly lower for CG (4.7) vs AL (5.9; averaged from 4.1 and 7.7 for the two independent runs). We observe similar wetting/dewetting fluctuation amplitudes in the CG and AL models, and the corresponding standard deviation values are 5.1 (CG) and 3.9 (AL). The AL results are in line with average and standard deviation values of 5.8 and 4.0 previously calculated in ref 3 using a smaller cavity−ligand simulation box (1030 vs 1950 water molecules) and mirrored cavities and ligands. These results indicate that the hydrophobic cavity is spontaneously undergoing wetting/dewetting transitions. However, we note that these transitions are faster for the CG model than the AL model.

Two general factors may influence the dynamics of dewetting: (1) the diffusion speed of the water molecules, which is 1.7 times larger for mW vs TIP4P water as inferred by comparison of their self-diffusion coefficients,[25] and (2) the existence of free energy barriers for the wetting/dewetting transition, the magnitude of which increases with the liquid−vapor surface tension γ_{lv}.[46,47] Figure 4a presents the liquid−vapor surface of water as a function of temperature computed

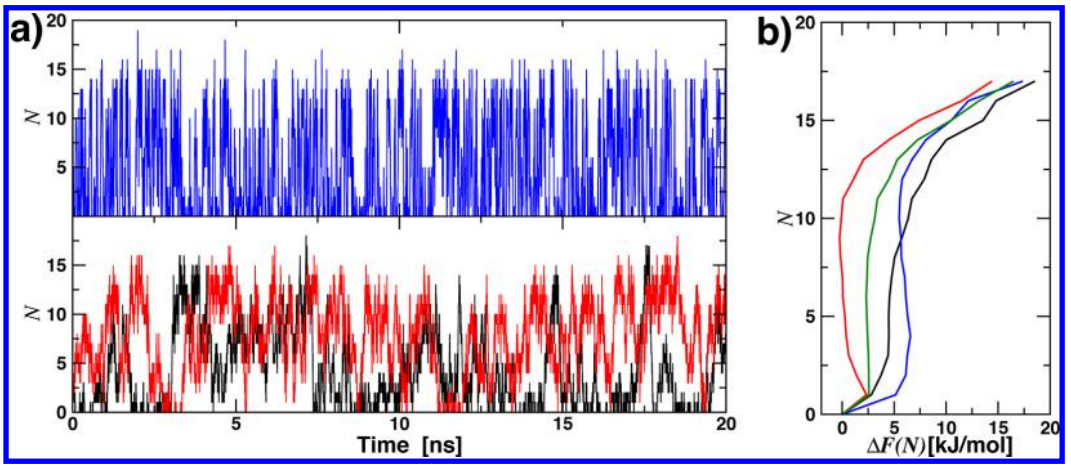

Figure 3. Comparison of the wetting/dewetting transitions of the hydrophobic cavity depending on the model resolution from simulations with the hydrophobic ligand placed in the bulk (ξ = 1.15 nm). (a) Time series of the number of water molecules inside the cavity from CG (blue) and two independent AL (black, red). The first 20 ns only out of a total of 50 ns are shown for the CG system. (b) Corresponding relative free energy profiles $F(N)$ obtained from the normalized probability distributions using the empty states $F(N = 0) = 0$ as a reference (see main text). The ensemble average free energy between the two AL runs is also shown (green).

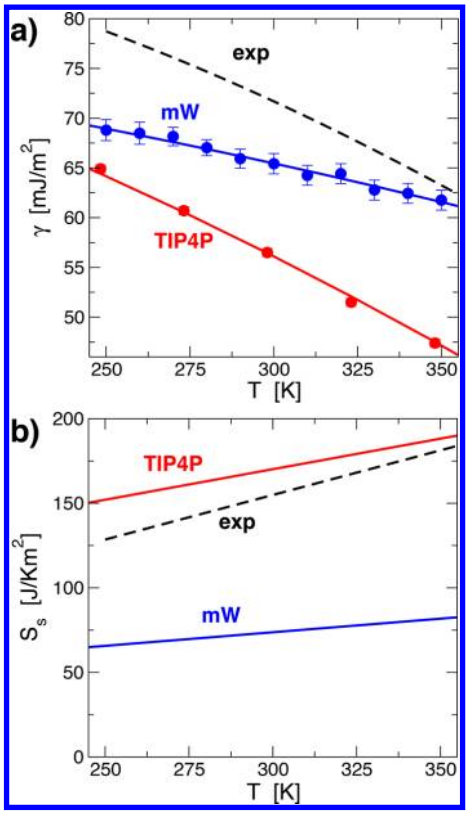

Figure 4. Surface properties of water. (a) Liquid−vapor surface tension and (b) surface entropy. Experimental data from ref 48. Calculated values for the TIP4P water model from ref 49. Data for the mW model were calculated in this work as described in the Molecular Models and Methods section.

for mW water in this work, along with experimental[48] and TIP4P water[49] results from the literature. The surface tension of mW at 298 K, γ_{lv} = 66 mJ/m^2,[25] is larger than for TIP4P, γ_{lv} = 56.5 mJ/m^2.[49,50] Thus, the larger characteristic time scale for the wetting/drying of the AL cavity suggests that the wetting/dewetting free energy barrier does not play a significant role in the dynamics.

To evaluate this hypothesis, we estimated for both CG and AL models the free energy profiles for hydrating the cavity, $F(N) = -k_B T \ln P(N)$, where k_B is Boltzmann's constant, T is the absolute temperature, and $P(N)$ is the probability of finding a number N of water of molecules inside the cavity (Figure 3b). These profiles are relative to a reference empty state, i.e., $F(N = 0) = 0$. For $3 \leq N \leq 10$, the free energy profiles are essentially flat. In the CG system, it is about 6 kJ mol^{-1} higher than for the empty cavity. Instead, in the AL system, this free energy is comparable to the thermal energy at 298 K, i.e., 2.5 kJ mol^{-1}, as previously reported.[22] This suggests a somewhat less favorable hydration propensity of the CG vs AL cavity system, consistent with the average occupancies reported above. However, cavity states with $N > 10$ become increasingly inaccessible, and the corresponding free energy profiles are virtually identical between the CG model and cumulative ensemble averages from the independent AL runs (Figure 3b, cf. blue and green lines). Similar maximum occupancies N = 19 (CG) and N = 18 (AL) are also observed for the two simulation models.

Overall, these free energy profiles display no sizable free energy barrier separating dry and hydrated cavity states (Figure 3b) and are consistent with the observation that a completely dry cavity is significantly more stable compared with a fully hydrated cavity.[22] The lack of such barriers allows us to conclude that the different time scales of the wetting/dewetting transitions in the CG and AL models are not controlled by the surface tension γ_{lv}, but instead by water mobility. In this respect, the wetting/dewetting behavior of Setny's cavity (0.8 nm radius, see Figure 1) contrasts with the sharp first-order like wetting/dewetting transitions observed for pairs of flat hydrophobic plates of similar size (0.88 nm radius) in mW water for which two well-defined dry and wet states exist separated by a barrier of 8.5 kJmol^{-1}.[33]

Correspondence of the maximum and minimum hydration states of the cavity is also of interest for the comparison between AL and CG model resolutions. Figure 5 shows

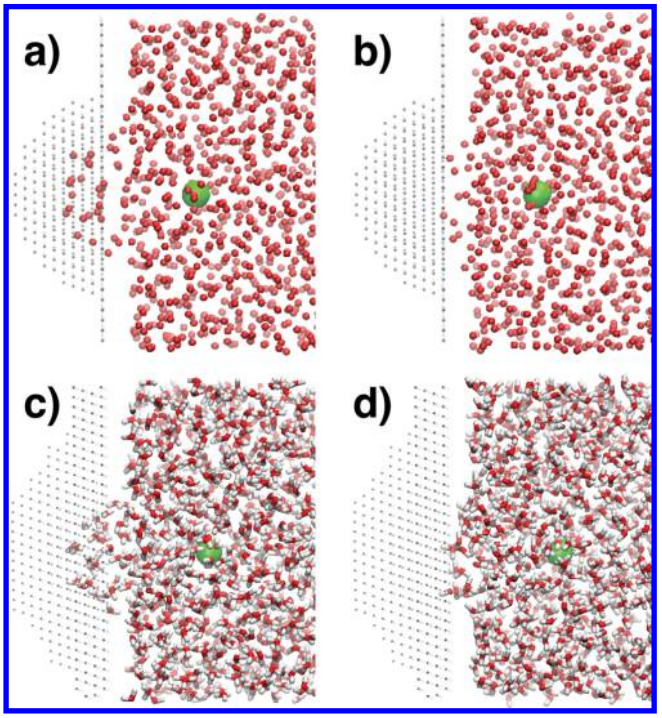

Figure 5. Hydration/dewetting of the hydrophobic cavity. Example snapshots from MD simulations for (a) maximum and (b) minimum water occupancies from CG simulation and (c) maximum and (d) minimum water occupancies from AL simulation. For graphical purposes, the location of the cavity and wall particles is indicated by dots. The ligand (L, green sphere) is located at the longest distance from the cavity considered for calculation of thermodynamic properties.

examples of MD snapshots for maximum and minimum hydration levels of the cavity when the ligand is at ξ = 1.15 nm. No relevant difference is observed when comparing CG and AL models. The same conclusion can be drawn when comparing the overall water density profiles in the simulated systems (not shown). We also analyzed the residual hydration in the two models, i.e., the hydration due to the water molecules inside the cavity in the bound state. The average number of water neighbors in the first solvation shell for these water molecules is 3.9 for the AL and 3.5 for the CG model. These results indicate that the residual water in the cavity is not vapor-like but rather is liquid protruding from the bulk into the cavity.

3.2. CG and AL Thermodynamics of Cavity−Ligand Binding. Figure 6 summarizes the thermodynamic signatures

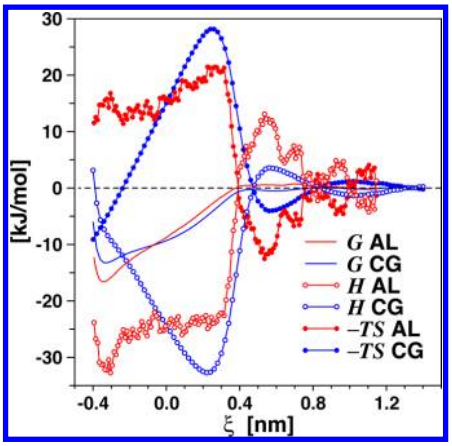

Figure 6. Thermodynamic signature profiles along the binding coordinate ξ for a hydrophobic ligand binding a hydrophobic cavity. Gibbs free energy, G, enthalpy, H, and entropic term, $-TS$, are shown as calculated from CG (blue) and AL (red) simulations. See Figure S2 in the Supporting Information for corresponding data on the temperature dependence of the free energy profiles. AL data correspond to refs 3 and 4.

Scheme 1. Thermodynamic Cycle for the Major Contributions to Cavity−Ligand Binding[a]

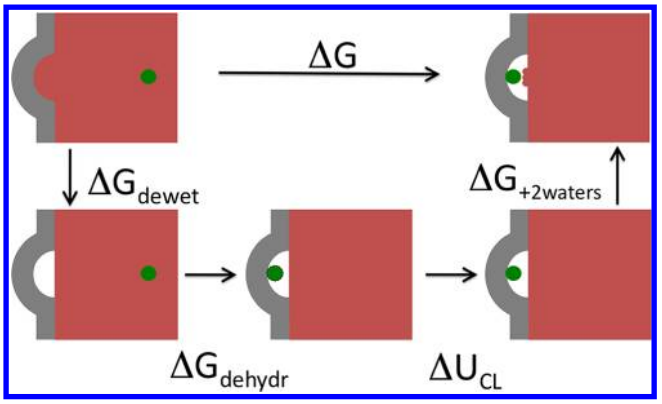

[a]This is a simplified representation for graphical purposes only to highlight the main contributions used for comparison between the two models and between simulations and experiments. First, the water leaves the cavity with the ligand in the bulk, contributing a free energy of cavity dewetting, ΔG_{dewet}. Second, the ligand dehydrates upon transfer from the bulk to the dry cavity, contributing a free energy of ligand dehydration, ΔG_{dehydr}. Third, the direct cavity−ligand interaction energy, ΔU_{CL}, is turned on. Fourth, about two water molecules are transferred from the bulk to the cavity occupied by the ligand and contribute to residual ligand hydration.

for hydrophobic cavity−ligand binding depending on model resolution. In both CG and AL models, the free energy profiles corresponding to the approach of the ligand from bulk water to the cavity, $G(\xi)$, is mostly flat until about 0.4 nm from the cavity wall. A similar slope is observed for the CG model in the range $0 < \xi < 0.4$ nm. In this range, free energy values for the CG model are about 1.5 kJ mol^{-1} smaller than for the AL model. However, this trend inverts once the ligand enters inside the cavity region ($\xi < 0$ nm). The total free energy changes upon binding, ΔG, are −13.2 (CG) and −16.5 (AL) kJ mol^{-1}. Importantly, the minima of the free energy profiles, which correspond to the bound state, ξ_B, in which the ligand is in contact with the cavity, are located at almost identical distances in the two models (CG, $\xi_B = -0.34$; AL, $\xi_B = -0.345$ nm).

The overall cavity−ligand binding free energy, ΔG, can be interpreted as the resulting balance of contributions of different natures that result from decomposing the binding process in a thermodynamic cycle (Scheme 1). First, the water leaves the cavity with the ligand deep in the bulk, contributing a free energy of cavity dewetting, ΔG_{dewet}. Second, the ligand dehydrates upon transfer from the bulk to the dry cavity, contributing a free energy of ligand dehydration, ΔG_{dehydr}. Third, the direct cavity−ligand interaction energy, ΔU_{CL}, is turned on. Fourth, about two water molecules are transferred from the bulk to the cavity occupied by the ligand, considering that we observe on average only ∼2.5 water molecules in the cavity in the bound state (Figure 2), compared with the ∼20 water molecules in the first hydration shell in the bulk. We assume the last term to be negligible for the comparison between AL and CG model resolutions. ΔU_{CL} is an additive force field term that can be extracted from the simulations. Thus, it is straightforward to represent the total ΔG of binding as a sum of terms corresponding to each cycle step. We examine these terms independently to verify if different/similar cavity−ligand binding propensities in the CG and AL models arise from the same physicochemical contributions, as opposed to unphysical error cancellation. Instead, it is not possible to do the same along the reaction coordinate ξ for the binding free energy and its enthalpy and entropy components, because the free energy contributions of dewetting and dehydration along the reaction coordinate are highly coupled.

The partial dehydration of the ligand upon binding, ΔG_{dehydr}, is the most sizable contribution to the free energy of cavity−ligand binding.[21] This quantity can be approximately related to the free energy of dehydration of the ligand, considering that we observe ∼2.5 water molecules in the cavity in the bound state (Figure 2 and Scheme 1), compared to ∼20 water molecules in the first hydration shell of methane in the bulk. The free energy of hydration of the M solute in mW water[32] and that of OPLS methane in TIP4P water[51,52] are 6.9 (CG) and 9.2 (AL) kJ mol^{-1}, respectively, at 298 K. These values are about 18% smaller (CG) and 9% larger (AL) than the experimental value (8.4 kJmol^{-1}). This indicates that the ΔG_{dehydr} contribution to cavity−ligand binding is comparatively less favorable in the CG vs AL system.

The second most important contribution to the binding free energy is the direct interaction energy between cavity and ligand, shown in Supporting Information Figure S3. There is a small difference in the cavity−ligand energies at the locus of binding; $\Delta U_{CL}(\xi_B)$ is −5.2 (CG) and −5.9 (AL) kJ mol^{-1}. This difference is due to the trimming in the numbers of paraffin layers on the back side of the cavity for the CG model. The number of paraffin particles in the wall of the cavity of the CG model was trimmed by about 20% to reduce computational costs, leading to a slightly less pronounced absolute minimum in the U_{CL} profile.

The third contribution to the free energy of binding, ΔG_{dewet}, takes into account the removal of water molecules exclusively from the cavity upon binding. Under the assumption that $\Delta G = \Delta U_{cl} + \Delta G_{dehydr} + \Delta G_{dewet}$, we estimate ΔG_{dewet} values of −1.1 (CG) and −1.4 (AL) kJ mol^{-1}, in line with what was previously reported for the AL model.[22] These ΔG_{dewet} values are consistent with the almost flat free energy profile observed for changing the occupancy of the cavity from ∼6 (unbound

state) to ∼2.5 (bound state) water molecules (Figure 4b) and significantly smaller than the corresponding ΔG_{dehydr} values.

Overall, our analysis indicates that the differences of cavity−ligand binding free energies observed between the CG and AL models arise largely from the fact that the ΔG_{dehydr} contribution to cavity−ligand binding is comparatively less favorable in the CG vs AL system. This accounts for a difference of ∼2.3 kJ mol^{-1}, which could be eliminated by a reparameterization of the hydration free energy of the methane in the two models to match the experimental value. The direct cavity−ligand energy, U_{CL}, accounts for a difference of ∼0.6 kJ mol^{-1}, and it is expected to disappear when using identical cavities in the CG and AL simulations. In the next part of this section, we show that although the dewetting, ΔG_{dewet}, has a negligible contribution to the overall hydrophobic binding free energy, it contributes significantly to the enthalpy and entropy signatures of the cavity−ligand binding process.

We estimated the enthalpy, $H(\xi)$, and entropy, $-TS(\xi)$, contributions to the free energy $G(\xi)$ at 298 K (Figure 6). This analysis is based on $G(\xi)$ curves at five different temperatures (see Supporting Information, Figure S4). Overall, it can be noticed that enthalpy and entropy profiles in the CG model are significantly smoother compared with the AL model. The major factor determining this difference is the different methodology employed to calculate $G(\xi)$ (see Molecular Models and Methods section). In addition, CG profiles were determined using more extensive simulation sampling and a finer discrete representation of the reaction coordinate.

The CG and AL thermodynamic signature profiles capture the qualitative characteristics of the binding process while the ligand is outside the cavity. When the ligand is inside the cavity, the two models present distinct enthalpy and entropy, as we explain below. The most relevant features in Figure 6 are (1) the initial full enthalpy−entropy compensation that results in an almost flat $G(\xi)$ for $0.4 < \xi < 1.4$ nm, (2) the maximum in enthalpy at $\xi \approx 0.5-0.6$ nm ($H(\xi)$ is 3.5 (CG) and 13 (AL) kJ mol^{-1}), (3) the maximum in entropy at $\xi \approx 0.2-0.3$ nm ($-TS(\xi)$ is 28 (CG) and 21 (AL) kJ mol^{-1}), and (4) the rapid exchange of entalpy−entropy compensating terms upon the (enthalpy-favored) expulsion of water molecules from the cavity. We note that while the AL model predicts an enthalpy-dominated bound state, opposed by entropy as a consequence of the removal of the solvent fluctuations in the system, the CG model predicts that the bound state is favored by both entropy and enthalpy.

We further compared the two models considering the entropy contributions for the three main processes shown in Scheme 1. The direct cavity−ligand interaction does not contribute to relative entropy changes along ξ, because both cavity and ligand atoms are kept at fixed positions during the simulations (CG, constrained; AL, restrained). The entropy change upon cavity−ligand binding results instead from two opposing contributions: (1) an *increase in entropy* due to the dehydration of the ligand (i.e., negative $-T\Delta S_{dehydr}$) and (2) a *decrease in entropy* due to the removal of high-entropy vapor-like solvent fluctuations upon cavity dewetting (i.e., positive $-T\Delta S_{dewet}$). The value of ΔS_{dehydr} of the M methane ligand in mW water is 40 JK^{-1} mol^{-1}.[52] This is comparable to the entropy of dehydration of OPLS methane in TIP4P water of about 47 JK^{-1} mol^{-1},[51] i.e., a $-T\Delta S_{dehydr}$ of about −13.95 kJ mol^{-1}. These contributions are just about 60% of the experimental value of 66.5 JK^{-1} mol^{-1} for the complete dehydration of methane in water.[51] Improved AL values of entropy of hydration can be achieved through reparametrization of the models for methane and water. Examples can be found in the recent work by Ashbaugh et al.[51] The entropy loss on hydration in the CG model, on the other hand, is limited by the intrinsic lack of rotational modes in the monatomic mW water model. The entropy of hydration of methane in the monatomic mW water model is in line with the theoretical prediction[53] that up to 40% of the hydration entropy of methane is due to orientational contributions to the ordering of water in the presence of methane, which are absent in the monatomic water model.

The formation of clathrate-like ordering of water around dissolved methane molecules has long been invoked as the rationale for explaining the decrease in entropy of water upon the hydration of methane.[54] It is worth noticing that the mW water model is—to our knowledge—the only coarse-grained model of water that was successfully used to investigate the nucleation and growth of clathrate hydrates,[30−32,34,55,56] the prototype of water-driven methane assembly. The tetrahedral interactions in the mW model allow capturing the expected entropy loss associated with the hydrophobic hydration of methane. Instead, the solvation of methane-like Lennard-Jones solutes in a Lennard-Jones solvent with the number density of liquid water produces an increase in entropy,[57] i.e., a sign of hydration entropy that is at odds with experimental results for hydrophobic solutes.

The entropic contributions of cavity dewetting were computed as the difference between the actual entropy of binding and the entropy of dehydration, $\Delta S_{dewet} = \Delta S - \Delta S_{dehydr}$. The entropy of dewetting is negative independently of the water model employed. On the other hand, the magnitude of ΔS_{dewet} is model specific. For the AL model, a large contribution from dewetting is observed ($-T\Delta S_{dewet} \approx 29$ kJ mol^{-1} at ξ_b). For the CG model, the contribution is significantly smaller ($-T\Delta S_{dewet} \approx 5$ kJ mol^{-1} at ξ_b). To understand this difference, we focus on the effect of the lack of rotational degrees of freedom on the entropy of dewetting. Cavity dewetting involves a decrease in the area of water exposed to a vacuum or the hydrophobic cavity. Therefore, the reduced entropy of dewetting of the CG model should be associated with a comparatively smaller surface entropy for the CG vs AL model. Data of the water surface entropy, minus the derivative of the liquid−vapor surface tension with temperature, is shown in Figure 4b for the mW and TIP4P models and from experimental results. The surface entropy of mW is about half of that for TIP4P water and experimental results (Figure 3b). A significant increase of rotational entropy occurs upon creation of a liquid−vapor surface in real water. This entropic effect is captured by a fully atomistic water model yet is absent in the monatomic one. It may be argued that cavity dewetting is better represented by a liquid−vapor transition and that the corresponding entropy change is also underestimated by a water model without rotational degrees of freedom. The strong undersestimation of the magnitude of the negative entropy change associated with cavity dewetting in the CG model results in a total positive entropy gain upon binding due to the positive (expected) entropy gain upon methane dehydration.

The major disagreement between the thermodynamic signatures for the two models is noticed when the ligand approaches the bound state. More work is needed to assess the origin of the discrepancy between the AL and CG model when the ligand is located inside the cavity.

4. CONCLUSIONS

We compared the thermodynamic signatures of the hydrophobic noncovalent binding between a hemispherical cavity and a ligand using two alternative simulation models at different resolutions: first, a coarse-grained (CG) model based on mW water and the methane-like M solute;[32] second, an atomic-level (AL) model based on the popular TIP4P water model[38] and the OPLS united-atom methane model.[39] We find that the CG model accurately reproduces, as a function of the cavity−ligand distance, (1) the water occupancy of the cavity, (2) the cavity−ligand potential of mean force and its temperature dependence, and (3) the major qualitative features of the thermodynamic signature for cavity−ligand association of the AL model. However, discrepancies were observed in the last part of the binding process. Namely, while the AL model predicts an enthalpy-dominated bound state, opposed by entropy as a consequence of the removal of the solvent fluctuations in the system, the CG model predicts that the bound state is favored by both entropy and enthalpy.

In agreement with previous work by Setny et al.,[3,21,22,24] we find that the free energy of binding in the AL and CG models is dominated by the free energy of dehydration of the ligand, and that this term is comparable in the CG and AL models. We note that both CG and AL models underestimate the enthalpy and entropy of dehydration; therefore, this match is partially fortuitous, because a monatomic water model is not expected to quantitatively reproduce the dehydration entropy. The second, trivial, contribution to the binding energy arises from the direct cavity−ligand interaction energy, which can be selected to be identical in the two models. Interestingly, for both models the dewetting of the cavity contributes less than 10% of the total binding energy. However, this is expected to strictly depend on the cavity shape and size; therefore, this term should not be neglected *a priori*. Moreover, albeit cavity dewetting displays a minor contribution to the binding, it dominates the enthalpy and entropy signatures,[3,4] modulating the temperature dependence of the free energy of binding. Overall, our study shows that CG simulations with the mW monatomic model of water provide a promising approach to capture the qualitative features of molecular recognition thermodynamics, including solvent fluctuations and enthalpy−entropy compensation.

In this context, the Setny's model cavity−ligand system is an ideal system to verify the correspondence of different models for a reliable description of molecular recognition (thermo)-dynamics, because ligand dehydration drives binding (i.e., free energy term),[3,21,22,24] while wetting/dewetting transitions modulate the corresponding thermodynamic signature (i.e., enthalpy and entropy). It is well-known that wetting/dewetting transitions can be captured by straightforward Lennard-Jones models.[58] Single-length scale isotropic coarse-grained models of water, however, fail to predict the underlying thermodynamic signatures of solvation. As an example, the temperature dependence of the excess free energy of solvation in Lennard-Jones liquids predicts the opposite sign of the entropy compared with that in water.[57] Instead, the mW water model, which includes anisotropic interactions that mimic hydrogen-bonding anisotropy, reproduces the experimental sign of the entropy and enthalpy for methane hydration. This is most relevant in hydrophobic assembly and clathrate nucleation.

The present study focused on hydrophobic association in an apolar cavity−ligand system. However, a future goal of CG applications is to expand its use in biologically relevant scenarios in which polar groups and ions play an important role. The mW model incorporates the anisotropy of the hydrogen-bonding interactions in water through short-range three-body potentials, resulting in a computational speedup of over 2 orders of magnitude compared with AL simulations that explicitly include approximate electrostatic interactions. Hydrophobic,[32,33] hydrophilic,[34,59] and ionic[60,61] solutes have been coupled with mW water using the short-range anisotropic interaction paradigm, which holds as well in the presence of solvated charged systems owing to the strong electrostatic screening in aqueous solutions. Other CG models introduce the anisotropy of water interactions by explicitly mimicking electrostatic polarizable interactions,[62−65] but at the cost of reduced computational time savings that generally drop to one order of magnitude only. Water screening effects have been recently described for the model cavity−ligand system of this study and are likely transferable to biological scenarios,[4] suggesting that future application of the mW paradigm will lead to a preferable compromise between computational efficiency and model reliability. Therefore, our study sets the basis for extending the use of the mW water model to complex biomolecular association and water-driven assembly along increasing spatiotemporal scales at convenient computational costs.

■ ASSOCIATED CONTENT

Ⓢ Supporting Information

Figure S1, representing the potential of mean force between a pair of methane molecules in water computer with the AL and CG models; Figure S2, representing a droplet of mW water molecules used to calculate the contact angle with a paraffin wall; Figure S3, direct cavity−ligand interaction energy; and Figure S4, reporting the temperature dependence of the free energy profiles at the CG and AL model resolution. This material is available free of charge via the Internet at http://pubs.acs.org.

■ AUTHOR INFORMATION

Corresponding Author

*E-mail: r.baron@utah.edu, Valeria.Molinero@utah.edu.

Notes

The authors declare no competing financial interest.

■ ACKNOWLEDGMENTS

The authors thank Piotr Setny for critical comments and suggestions. This work was supported by startup funds from the Department of Medicinal Chemistry and from The University of Utah (R.B.) and by the National Science Foundation through CHE-1012651 (V.M.). We acknowledge the Center of High Performance Computing at The Univerisity of Utah for technical support and allocation of computer time.

■ DEDICATION

We congratulate Wilfred van Gunsteren on the occasion of his 65th birthday and thank him for his inspiration on the relevance of water modeling. R.B. thanks Wilfred for providing outstanding training during his doctoral work.

■ REFERENCES

(1) van Gunsteren, W.; Berendsen, H. J. C. *J. Mol. Biol.* **1984**, *176*, 559−564.

(2) van Gunsteren, W.; Berendsen, H. J. C. *Proc. Natl. Acad. Sci. U.S.A.* **1983**, *80*, 4315−4319.
(3) Setny, P.; Baron, R.; McCammon, J. A. *J. Chem. Theory. Comput.* **2010**, *6*, 2866−2871.
(4) Baron, R.; Setny, P.; McCammon, J. A. *J. Am. Chem. Soc.* **2010**, *132*, 12091−12097.
(5) Hummer, G. *Nat. Chem.* **2010**, *2*, 906−907.
(6) Michel, J.; Tirado-Rives, J.; Jorgensen, W. L. *J. Am. Chem. Soc.* **2009**, *131*, 15403−15411.
(7) Abel, R.; Young, T.; Farid, R.; Berne, B. J.; Friesner, R. A. *J. Am. Chem. Soc.* **2008**, *130*, 2817−2831.
(8) Baron, R.; Setny, P.; McCammon, J. A., Hydrophobic Association and Vol.-Confined Water Molecules. In *Protein-Ligand Interactions*; Gholke, H., Ed.; Wiley-VCH: New York, 2012; in press.
(9) Berne, B. J.; Weeks, J. D.; Zhou, R. *Annu. Rev. Phys. Chem.* **2009**, *60*, 85−103.
(10) Rasaiah, J. C.; Garde, S.; Hummer, G. *Annu. Rev. Phys. Chem.* **2008**, *59*, 713−740.
(11) Dunitz, J. *Chem. Biol.* **1995**, *2*, 709−712.
(12) Dunitz, J. *Science* **1994**, *264*, 670−670.
(13) Yin, H.; Hummer, G.; Rasaiah, J. C. *J. Am. Chem. Soc.* **2007**, *129*, 7369−7377.
(14) Cooper, A. *Biophys. Chem.* **2005**, *115*, 89−97.
(15) van Gunsteren, W. F.; Bakowies, D.; Baron, R.; Chandrasekhar, I.; Christen, M.; Daura, X.; Gee, P.; Geerke, D. P.; Glattli, A.; Hünenberger, P. H.; Kastenholz, M. A.; Oostenbrink, C.; Schenk, M.; Trzesniak, D.; van der Vegt, N. F.; Yu, H. B. *Angew. Chem., Int. Ed.* **2006**, *45*, 4064−4092.
(16) Winger, M.; Trzesniak, D.; Baron, R.; van Gunsteren, W. F. *Phys. Chem. Chem. Phys.* **2009**, *11*, 1934−1941.
(17) Baron, R.; de Vries, A. H.; Hünenberger, P. H.; van Gunsteren, W. F. *J. Phys. Chem. B* **2006**, *110*, 8464−8473.
(18) Baron, R.; de Vries, A. H.; Hünenberger, P. H.; van Gunsteren, W. F. *J. Phys. Chem. B* **2006**, *110*, 15602−14.
(19) He, X.; Shinoda, W.; DeVane, R.; Klein, M. L. *Mol. Phys.* **2010**, *108*, 2007−2020.
(20) Baron, R.; Trzesniak, D.; de Vries, A. H.; Elsener, A.; Marrink, S. J.; van Gunsteren, W. F. *ChemPhysChem* **2007**, *8*, 452−61.
(21) Setny, P. *J. Chem. Phys.* **2007**, *127*, 054505.
(22) Setny, P.; Geller, M. *J. Chem. Phys.* **2006**, *125*, 144717.
(23) Setny, P.; Wang, Z.; Cheng, L.; Li, B.; McCammon, J. *Phys. Rev. Lett.* **2009**.
(24) Setny, P. *J. Chem. Phys.* **2008**, *128*, 125105.
(25) Molinero, V.; Moore, E. B. *J. Phys. Chem. B* **2009**, *113*, 4008−4016.
(26) Vega, C.; Abascal, J. L. *Phys. Chem. Chem. Phys.* **2011**, *13*, 19663−88.
(27) Moore, E. B.; Molinero, V. *J. Chem. Phys.* **2009**, *130*, 244505.
(28) Moore, E. B.; Molinero, V. *J. Chem. Phys.* **2010**, *132*, 244504.
(29) Moore, E. B.; Molinero, V. *Nature* **2011**, *479*, 506.
(30) Jacobson, L. C.; Hujo, W.; Molinero, V. *J. Am. Chem. Soc.* **2010**, *132*, 11806.
(31) Jacobson, L. C.; Matsumoto, M.; Molinero, V. *J. Chem. Phys.* **2011**, *135*, 074501.
(32) Jacobson, L. C.; Molinero, V. *J. Phys. Chem. B* **2010**, *114*, 7302−7311.
(33) Xu, L.; Molinero, V. *J Phys Chem B* **2010**, *114*, 7320.
(34) Jacobson, L. C.; Hujo, W.; Molinero, V. *J. Phys. Chem. B* **2010**, *114*, 13796.
(35) Shimizu, S.; Chan, H. *J. Chem. Phys.* **2000**, *113*, 4683.
(36) Molinero, V.; Goddard, W. A., III. *J. Phys. Chem. B* **2004**, *108*, 1414.
(37) Pascal, T. A.; Goddard, W. A.; Jung, Y. *Proc. Natl. Acad. Sci. U.S.A.* **2011**, *108*, 11794.
(38) Jorgensen, W. L.; Chandrasekhar, J.; Madura, J. D.; Impey, R. W.; Klein, M. L. *J. Chem. Phys.* **1983**, *79*, 926.
(39) Jorgensen, W. L.; Madura, J. D.; Swenson, C. J. *J. Am. Chem. Soc.* **1984**, *106*, 6638.
(40) Stillinger, F. H.; Weber, T. A. *Phys. Rev. B* **1985**, *31*, 5262.
(41) Plimpton, S. *J. Comput. Phys.* **1995**, *117*, 1.
(42) Hockney, R. W. *Methods Comput. Phys.* **1970**, *9*, 136.
(43) Hoover, W. *Phys. Rev. A* **1989**, *40*, 2814.
(44) Nosé, S. *J. Chem. Phys.* **1984**, *81*, 511.
(45) Brooks, B. R.; Brooks, C. L., 3rd; Mackerell, A. D., Jr.; Nilsson, L.; Petrella, R. J.; Roux, B.; Won, Y.; Archontis, G.; Bartels, C.; Boresch, S.; Caflisch, A.; Caves, L.; Cui, Q.; Dinner, A. R.; Feig, M.; Fischer, S.; Gao, J.; Hodoscek, M.; Im, W.; Kuczera, K.; Lazaridis, T.; Ma, J.; Ovchinnikov, V.; Paci, E.; Pastor, R. W.; Post, C. B.; Pu, J. Z.; Schaefer, M.; Tidor, B.; Venable, R. M.; Woodcock, H. L.; Wu, X.; Yang, W.; York, D. M.; Karplus, M. *J. Comput. Chem.* **2009**, *30*, 1545.
(46) Huang, X.; Margulis, C. J.; Berne, B. J. Dewetting-induced collapse of hydrophobic particles. *Proc. Natl. Acad. Sci. U. S. A.* **2003**, *100*, 11953−11958.
(47) Lum, K.; Chandler, D. *Int. J. Thermophys.* **1998**, *19*, 845.
(48) Floriano, M. A.; Angell, C. A. *J. Phys. Chem.* **1990**, *94*, 4199.
(49) Sakamaki, R.; Sum, A. K.; Narumi, T.; Yasuoka, K. *J. Chem. Phys.* **2011**, *134*, 124708.
(50) Chen, F.; Smith, P. E. *J. Chem. Phys.* **2007**, *126*, 221101.
(51) Ashbaugh, H. S.; Collett, N. J.; Hatch, H. W.; Staton, J. A. *J. Chem. Phys.* **2010**, *132*, 124504.
(52) Spencer, J. E.; Baron, R.; Molinero, V. In preparation.
(53) Kinoshita, M.; Matubayasi, N.; Harano, Y.; Nakahara, M. *J. Chem. Phys.* **2006**, *124*, 024512.
(54) Stillinger, F. *Science* **1980**, *209*, 451.
(55) Jacobson, L.; Hujo, W.; Molinero, V. *J. Phys. Chem. B* **2009**, *113*, 10298.
(56) Jacobson, L. C.; Molinero, V. *J. Am. Chem. Soc.* **2011**, *133*, 6458.
(57) Lynden-Bell, R. M.; Giovambattista, N.; Debenedetti, P. G.; Head-Gordon, T.; Rossky, P. J. *Phys. Chem. Chem. Phys.* **2011**, *13*, 2748.
(58) Bolhuis, P. G.; Chandler, D. *J. Chem. Phys.* **2000**, *113*, 8154.
(59) Le, L.; Molinero, V. *J. Phys. Chem. A* **2010**, *115*, 5900.
(60) DeMille, R.; Cheatham, T., III; Molinero, V. *J. Phys. Chem B* **2011**, *115*, 132.
(61) DeMille, R. C.; Molinero, V. *J. Chem. Phys.* **2009**, *131*, 034107.
(62) Ichiye, T.; Tan, M. *J. Chem. Phys.* **2006**, *124*, 134504.
(63) Riniker, S.; van Gunsteren, W. F. *J. Chem. Phys.* **2011**, *134*, 084110.
(64) Wu, Z.; Cui, Q.; Yethiraj, A. *J. Phys. Chem. B* **2010**, *114*, 10524.
(65) Yesylevskyy, S. O.; Schäfer, L. V.; Sengupta, D.; Marrink, S. J. *PLoS Comp. Biol.* **2010**, *6*, e1000810.